# *Ab initio* calculation of the depth-dependent optical reflectance from layer-by-layer atomic disorder

**Sean M. Anderson[1], Bernardo S. Mendoza[*,1], Ramón Carriles[1]**

[1] Centro de Investigaciones en Óptica, A.C., León, Guanajuato 37150, Mexico

Received XXXX, revised XXXX, accepted XXXX
Published online XXXX

**Key words:** reflectance spectroscopy, atomic disorder, CAP, surface, strain

[*] Corresponding author: e-mail bms@cio.mx, Phone: +52-477-4414200, Fax: +52-477-4414209

We present a simple model to study the effects of displacing a single atomic monolayer on the linear optical properties of a material. As an example, we calculate the change in reflectance of a Si(111)(1×1):H slab after disordering successively deeper atomic layers. We find that the reflectance varies significantly at photon energies above 2.0 eV, and that the disordered slab produces a larger reflectance than the relaxed slab. The results also show a quantitative difference in the contribution from the odd and even atomic layers to the calculated reflectance. This simplified model is a first approach; also, it can be extended to consider more realistic systems that can be probed by techniques such as coherent acoustic phonon (CAP) spectroscopy, and can also be applied to two-dimensional materials.



**1 Introduction** The characterization and profiling of inhomogeneities in solid state materials has become increasingly important for the development of new and improved optoelectronic technologies. This includes, but is not restricted to, studying the effects of defects or impurities on the local optical properties of the host materials, as well as determining specific defect profiles. While some of the existing techniques are destructive, optical methods are non-invasive and usually work in situ; thus, it is desirable to develop these tools in order to better analyze the optical response of a given material. These experimental studies should be coupled with the necessary theoretical framework to support the observations. Namely, *ab initio* calculations can yield frequency-dependent optical functions that take into account any lattice disorder, strain, inhomogeneities or defects that may be present. The calculation of the linear optical properties from both surface and bulk regions [1–7] is now computationally efficient and numerically more accurate than the traditional phenomenological or Maxwell models often found in the literature. This enables an in-depth profiling of the interactions between structural characteristics and the local optoelectronic properties of a given material.

To this end, we have developed a simple model to study the effects of atomic disordering in a sample surface-bulk system. In this model, we move the $z$-coordinate for each individual atom, one at a time, away from the equilibrium position in small, uniform translations, starting from the surface layer down into the bulk. Since the unit cell is repeated along the $xy$ plane, this is equivalent to translating individual monolayers within the structure. The linear optical response function can then be calculated for the entire structure, taking into account the newly disordered atomic positions. Although this proposed model is an oversimplification of the real physical response of the material, it is a first building block for more sophisticated theoretical treatments. In particular, once the individual monolayer responses to the lattice deformations are known, it should be possible to calculate the induced strain response for a specific slab or surface. The generated strain need not be uniform, as it could also be any arbitrary material deformation induced by a traveling wave or another excitation, such as

the one induced in a coherent acoustic phonon (CAP) experiment.

CAP spectroscopy (also called picosecond ultrasonics) is an acousto-optical technique that is well suited for these kinds of measurements. It is a pump-probe technique [8–12] that involves an ultrafast, high-intensity *pump* pulse impinging on an absorbing material, and a second *probe* pulse that senses changes in the optical properties of the material that are induced by the pump pulse. The pump pulse is absorbed at the surface, establishing a transient strain wave at the sample surface that traverses the material as a longitudinal acoustic phonon. This CAP wave acts as a localized strained layer that moves down into the material at the material-specific phonon velocity. It modifies the local dielectric constants, creates discontinuities, and causes a periodic modulation of the optical properties. The CAP wave effectively samples different layers as it travels through the material, which positions it as a promising non-invasive option for measuring optical properties as a function of depth and across material interfaces, as well as being sensitive to lattice deformation and inhomogeneities. In particular, the technique has been extensively used to study the structural properties of metals [13,14], semiconductors [15–21], and transition metal oxysalts [22–26]. Likewise, it has been shown to be an effective tool for determining thin film thicknesses [27,28], elasto-mechanical [29,30, 13,31] and optical properties [32,17,19], low-frequency phonon dispersion and attenuation mechanisms [33,34], buried interface roughness [35], inhomogeneities in disordered films [27], doping profiles [21], lattice defects [36–39], and shear strain waves using time-resolved polarization measurements [40,41].

Our model could help in the understanding of the experiments based on techniques such as CAP or reflectance anisotropy spectroscopy (RAS). There are some available *ab initio* calculations applied towards studying CAP spectroscopy [42,36], but we consider that there is room for more theoretical development in this area. Accordingly, we have developed our model with some of the basic characteristics from these types of experiments. The interatomic displacements that we consider in our model (up to 0.224 Å) are of the same order as those induced in real samples during a CAP experiment [42]. The spatial resolution of CAP is on the order of 100 Å [9], while RAS can probe only a few monolayers on the surface, and current *ab initio* methods are very well suited for analysis at this scale [43,44]. These considerations result in calculated reflectivity changes (described in Sec. 3) that are within the detection sensitivity range accessible with lock-in techniques [38]. We consider that our model manages to yield relevant insight about strain waves in surface-bulk systems, and helps elucidate the physical phenomena dictating the observed changes in reflectance. Additionally, our model can be easily applied towards the study of two-dimensional materials, which have very promising optoelectronic properties.

This paper is organized as follows. In Sec. 2, we present the relevant equations and theory that describe the calculation of the linear optical response and the reflectance difference spectrum. In Sec. 3, we present and analyze the calculated reflectance using the Si(111)(1×1):H surface as a test case. Finally, we list our conclusions and final remarks in Sec. 4.

**2 Theory** To model a semi-infinite crystal, we utilize a slab, consisting of $N$ atomic layers and thickness $D$ inside a supercell of total height $L$, that includes the vacuum region required when using the repeated slab scheme, and is large enough to avoid the wave function tunneling to neighboring supercells [4]. The surface is parallel to the $xy$ plane, with the surface normal in the $z > 0$ direction. Following Ref. [4], the reflectance difference spectrum $\Delta R$ is defined as

$$\Delta R = \left.\frac{R_x + R_y}{2}\right|_{\text{relaxed}} - \left.\frac{R_x + R_y}{2}\right|_{\text{perturbed}}, \quad (1)$$

where $R_{\rm a}$ ($\rm a = \it x$ or $y$) is the normal incident reflectance for linearly polarized light in the $\hat{\mathbf{a}}$ direction. As explained in the introduction, our idea is to move the atoms of the slab away from their equilibrium positions, calculate $R_{\rm a}$ for this perturbed slab, and study the difference with the value of the unperturbed or relaxed structure via $\Delta R$. $R_{\rm a}$ can be calculated through the optical response of the slab system [45] as

$$R_{\rm a} = 4\left(\frac{\omega}{c}\right)\text{Im}\left[\frac{(D/2)\chi^{\rm aa}_{sc}(\omega)}{\boldsymbol{\chi}_b(\omega)}\right], \quad (2)$$

where $\omega$ is the angular frequency of the normally incident light impinging from the vacuum side, $c$ is the speed of light, $D/2$ is the half-slab thickness, $\boldsymbol{\chi}_{sc}(\omega)$ is the linear susceptibility for the supercell system, and $\boldsymbol{\chi}_b(\omega)$ is the linear susceptibility of the isotropic bulk crystal.

Within the usual independent-particle framework [6], we have that

$$\chi^{\rm aa}(\omega) = \frac{e^2}{\hbar}\int\frac{d\mathbf{k}}{8\pi^3}\sum_{vc}\frac{1}{\omega_{cv}(\mathbf{k})}\text{Im}\left[v^{\rm a}_{cv}(\mathbf{k})r^{\rm a}_{vc}(\mathbf{k})\right] \times\left(\frac{1}{\omega_{cv}(\mathbf{k})-\omega-i\eta}+\frac{1}{\omega_{cv}(\mathbf{k})+\omega+i\eta}\right), \quad (3)$$

with $\hbar\omega_n(\mathbf{k})$ being the energy of the electronic band $n$ at point $\mathbf{k}$ in the irreducible Brillouin zone, $\omega_{nm}(\mathbf{k}) = \omega_n(\mathbf{k}) - \omega_m(\mathbf{k})$; $n, m = v$ corresponds to a valence band, and $n, m = c$ is a conduction band. Here, $\mathbf{v}_{nm}(\mathbf{k})$ and $\mathbf{r}_{nm}(\mathbf{k})$ are the matrix elements of the electron velocity and position operators, with $\rm a = \it x$ or $y$. Lastly, $\eta$ can be used to include the broadening of the electronic levels. Many-body interactions can be included in an approximate manner using a scissors operator approach in Eq. (3), following Ref.

[46]. In this way, we adjust the calculated energy band gap to the correct experimental value. In Eq. (3), the first energy denominator includes the *resonant* terms, while the second denominator includes the *nonresonant* terms. Indeed, by taking $\eta \to 0$, we obtain Dirac delta functions $\delta(\omega_{cv}(\mathbf{k})-\omega)$ for the resonant term, and $\delta(\omega_{cv}(\mathbf{k})+\omega)$ for the nonresonant term. For positive energies, only the resonant term will contribute to $\chi^{\mathrm{aa}}(\omega)$, whereas the nonresonant term will yield zero contribution. As shown in Ref. [6], both terms are needed to accurately calculate $\chi^{\mathrm{aa}}(\omega)$. The bulk susceptibility, $\boldsymbol{\chi}_b(\omega)$, is obtained by using a bulk unit cell in Eq. (3); likewise, $\boldsymbol{\chi}_{sc}(\omega)$ is obtained by using a supercell, where it must be properly normalized with respect to the vacuum included in the total supercell height $L$ [7]. Then, we take $\boldsymbol{\chi}_{sc}(\omega) \to (L/D)\boldsymbol{\chi}_{sc}(\omega)$, so that even if a larger vacuum region is included, the results remains invariant.

**3 Results** We chose the Si(111)(1×1):H surface as a representative test case for our model. The ideal Si(111) bulk terminated surface has an unsaturated dangling bond at each of its surface Si atoms; the addition of an H atom at each surface will passivate this bond and yield an unreconstructed surface with a 1×1 unit cell. In this example, this surface is represented by a centrosymmetric slab of 38 atoms comprised of 36 Si atoms between one H atom on each surface; Fig. 1 presents a graphical representation of this slab. The hexagonal symmetry of this surface is such that $\chi^{xx}_{sc}(\omega) = \chi^{yy}_{sc}(\omega)$, and so, $R_x = R_y$. Choosing a centrosymmetric slab allows us to carry out the analysis over only half of the slab, since the other half yields identical results. The self-consistent ground state and the Kohn-Sham states needed in Eq. (3), along with the atomic positions for the relaxed slab, were calculated in the DFT-LDA framework using the plane-wave ABINIT code [47,48]. See Ref. [43] for a detailed account of this calculation. We found converged results for the surface $\boldsymbol{\chi}_{sc}(\omega)$ calculation using 244 $\mathbf{k}$ points and a cutoff energy of 7 Ha; 3107 $\mathbf{k}$ points and a cutoff energy of 10 Ha were used for the bulk $\boldsymbol{\chi}_b(\omega)$ calculation. A scissors shift of 0.7 eV was used for the surface, obtained from $G_0W_0$ calculations [52]. For the bulk, we applied a scissors shift of 0.98 eV in order to adjust the calculated direct band gap to the experimental value [49].

To identify which atom will be displaced, we tag each one in consecutive order starting at the surface, i.e. $H_1$ and $Si_2$ down to $Si_{19}$ (see Fig. 1). We can see that the odd Si atoms have the vertical bonds going down and the slanted bonds going up, and vice versa for the even Si atoms. We displace any given atom *up* (towards $z > 0$) or *down* (towards $z < 0$) by a percentage $p$ of the $z$ distance between atoms $Si_2$ and $Si_3$, which is 0.784 Å. We perturb only a single atomic monolayer at a time from its equilibrium position; all other atoms remain at their original (relaxed) positions. We restrict the present study to photon energies that are in the visible range; the experiments are much easier to perform, and there is no absorption of

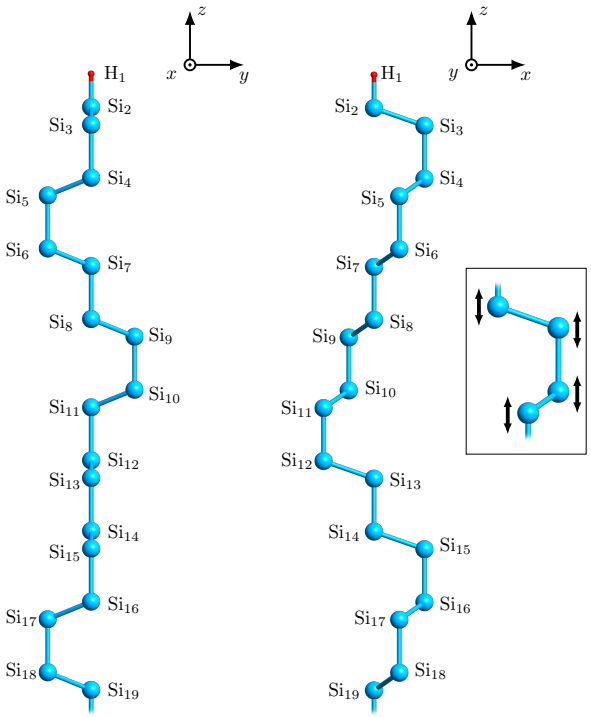


**Figure 1** $xz$ and $yz$ plane views of the relaxed Si(111)(1×1):H half-slab used in this work. All atoms (balls) are tagged according to their $z$ position within the slab. Each atom is connected to another via vertical or slanted bonds, represented by interconnecting rods. The inset to the right depicts the $z$ displacement that was carried out on each atom (and the corresponding monolayer), one at a time.

light as $\mathrm{Im}[\boldsymbol{\chi}_{(sc,b)}(\omega) = 0]$ in this range, since the direct band gap energies, besides being very similar for surface and bulk, are around 3.05–3.4 eV [49–52].

In Fig. 2, we present $\Delta R$ vs. $\hbar\omega$ for a $p = 30\%$ (0.224 Å) *up* or *down* displacement of selected $Si_n$ atoms. From the plot, we can see that $\Delta R \sim 0$ for energies below 2.0 eV; above this value, $\Delta R$ goes monotonically to more negative values, which implies that the perturbed structure reflects more light than the relaxed structure. We can also appreciate how the $\Delta R$ spectra can be grouped into the odd and even displaced $Si_n$ atoms. For the even $Si_{2n}$ atoms, $|\Delta R|$ is larger (smaller) than for the odd $Si_{2n+1}$ atoms, for *up* (*down*) displacements.

From this grouping, we can observe the influence of the vertical and slanted bonds on $\Delta R$. When displacing each atom in the *up* direction, the vertical bonds on the even (odd) Si atoms are compressed (elongated) while the slanted bond is elongated (compressed), and vice versa for the *down* displacement. This trend for $\Delta R$ reverses between the *up* and *down* displacements, and the even and odd Si atoms; thus, displacing an even atom *down* is similar to displacing an odd atom *up* and vice versa. This behavior is consistent with the fact that the bond geometry is

reversed from one case to the other; however, the surface breaks the symmetry along $z$, creating quantitative differences in $\Delta R$. Note that for normal incidence, the slanted bonds yield a significantly larger contribution to the linear optical properties over the vertical bonds.

To proceed with the analysis, in Fig. 3 we plot $\Delta R$ vs. atom position for a fixed energy of $\hbar\omega = 2.6$ eV, for values of $p$ between 5–30% in steps of 5%, which is equivalent to displacements between 0.040–0.224 Å in increments of 0.040 Å. In Fig. 3a, we present the odd ($H_1$, $Si_{2n+1}$) atoms displaced *down*. For $p = 5\%$, $\Delta R$ remains identical for every atom displacement. As $p$ increases, $\Delta R$ becomes increasingly negative, indicating again that the perturbed surface has a higher reflectance than the relaxed surface. $\Delta R$ is always zero for $H_1$ displacements, which is expected from the fact that the H atom quenches the surface states, making it optically inactive. It is interesting to note that as atoms that are farther away from the surface are displaced, $\Delta R$ reaches a constant value; as the displacement ($p$) increases, it takes deeper displacements to reach that value. This indicates that displaced atoms closer to the surface can be discerned by the changes in $\Delta R$, while displacements occurring towards the bulk of the material would be difficult to identify individually. In turn, this could be explained from the fact that the atoms located beyond the influence of the surface will all have the same effect on $\Delta R$, regardless of their exact depth within the bulk of the material. In Fig. 3b, we present $\Delta R$ for the same values

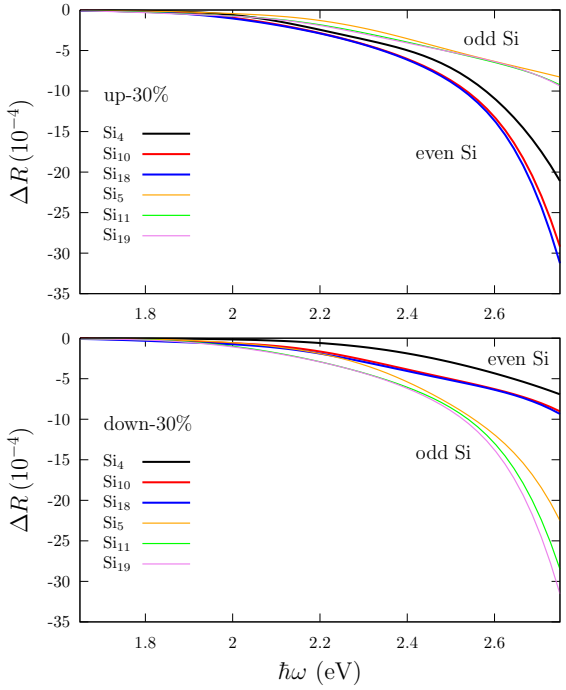


**Figure 2** $\Delta R$ vs. $\hbar\omega$ for a $p = 30\%$ (0.224 Å) *up* or *down* displacement of selected even and odd Si atoms.

of $p$ for even ($Si_{2n}$) atoms, displaced *up*. As discussed above in connection with Fig. 2, this *up* displacement of the even atoms is similar to the *down* displacement of the odd atoms; thus, the qualitative similarities between the results in Figs. 3a and 3b further confirm this fact. Likewise, we present *up* displacements for the odd atoms in Fig. 3c, and *down* displacements for the even atoms in Fig. 3d. The qualitative description of these results is similar to our comments above concerning Figs. 3a and 3b. However, we find that $\Delta R$ is about half the value presented in those figures, which is again in agreement with Fig. 2. In summary, we find that $\Delta R$ for atoms displaced *down* is larger for odd ($Si_{2n+1}$) atoms than for even ($Si_{2n}$) atoms, as shown in Figs. 3a and 3d. Likewise, we also find that displacing the even atoms *up* produces a larger $\Delta R$ than the odd atoms, as can be seen from Figs. 3b and 3c.

Lastly, in Fig. 4 we show $\Delta R$ vs. the atom position for different values of $\hbar\omega$, for a $p = 30\%$ *down* displacement only. The top panel shows the odd ($H_1$, $Si_{2n+1}$) atoms, while the bottom panel shows the even ($Si_{2n}$) atoms. Again, we see lower values for $\Delta R$ produced by displacing the even atoms than by displacing the odd atoms. $\Delta R$ remains zero for $\hbar\omega = 1.8$ eV, but as $\hbar\omega$ increases, $\Delta R$ grows increasingly negative; as before, this is in accordance with the results discussed in Fig. 2. We note that equivalent results were obtained for the *up* displacement as a function of $\hbar\omega$, but are not included here. Most importantly, Fig. 4 shows conclusive evidence that changes in $\Delta R$ can be used to monitor vertical displacements of atoms close to the surface, particularly at higher energies in the visible range.

We propose the following explanation for the calculated changes in reflectance. For an *up* (*down*) displacement, the even (odd) atoms will have elongated slanted bonds; for an *up* (*down*) displacement, the odd (even) atoms will have compressed slanted bonds. If we consider the response of the bonds as linear harmonic oscillators, an electron in an elongated bond will have a looser confinement compared to that in a compressed bond. This means that the electron potential for the elongated (compressed) bond has a lower (higher) curvature as compared to that of the relaxed bond, implying that the resonant frequency, being proportional to the curvature, is lower (higher) than for the relaxed bond. Therefore, the elongated (compressed) bond has a higher (lower) polarizability, which leads to a larger (smaller) increase in the reflectance.

Overall, our simple model for layer-by-layer atomic disordering verifies that detectable changes on the order of $10^{-4}$ occur to $\Delta R$, even when considering relatively small ($< 0.224$ Å) single-atom displacements. It is also capable of elucidating the mechanism behind the changes in reflectance; namely, the compression and elongation of the slanted Si bonds present in the Si(111)(1×1):H slab. We consider that an extension of this model, with a more accurate modeling of atomic disorder caused by a strain wave,

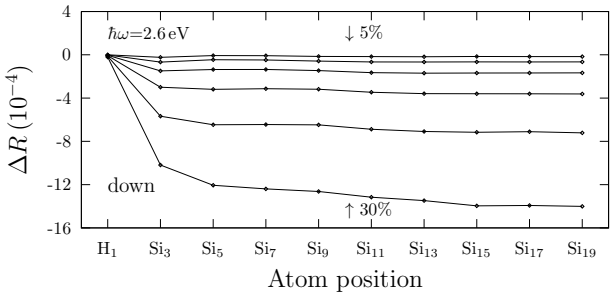


a) Odd atomic layers, displaced *down*.

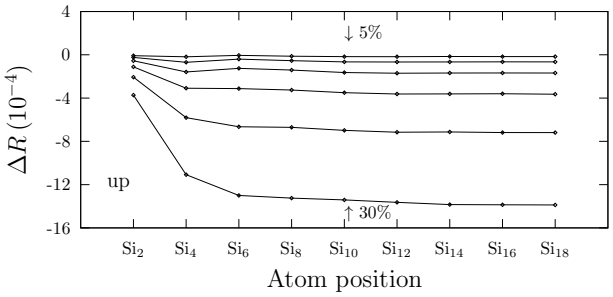


b) Even atomic layers, displaced *up*.

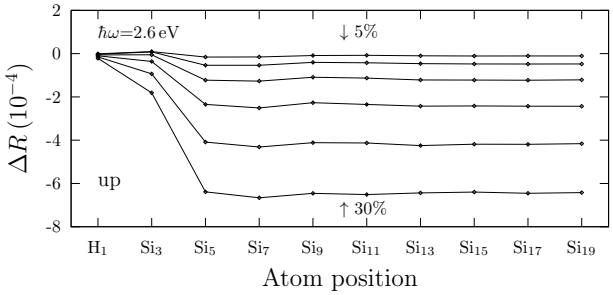


c) Odd atomic layers, displaced *up*.

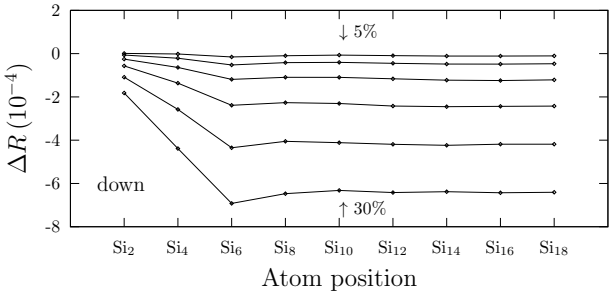


d) Even atomic layers, displaced *down*.

**Figure 3** $\Delta R$ vs. atom position (black dots) at $\hbar\omega = 2.6\,\text{eV}$, for values of $p$ between 5–30% in steps of 5%. Solid lines are for ease of viewing. Panel (a): odd ($H_1$, $Si_{2n+1}$) atoms displaced *down*. Panel (b): even ($Si_{2n}$) atoms displaced *up*. Panel (c): odd ($H_1$, $Si_{2n+1}$) atoms displaced *up*. Panel (d): even ($Si_{2n}$) atoms displaced *down*.

can be readily applied to study CAP experiments at the *ab initio* level for any crystalline semiconductor.

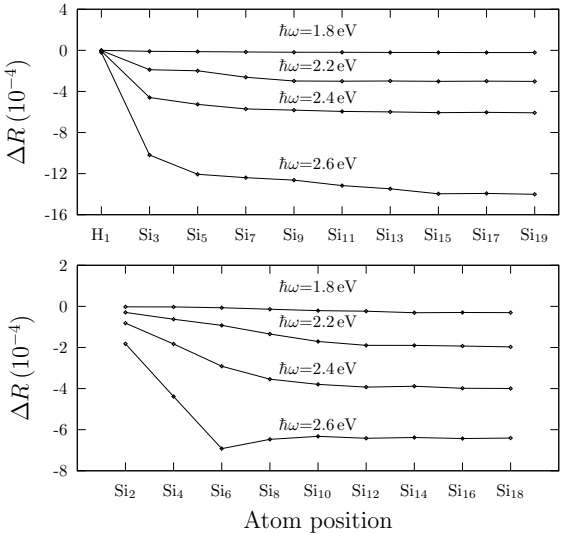


**Figure 4** $\Delta R$ vs. the atom position for different values of $\hbar\omega$, for atoms displaced *down* by $p = 30\%$. Odd ($H_1$, $Si_{2n+1}$) atoms are presented in the the top panel, and even ($Si_{2n}$) atoms in the bottom panel. The solid lines are for ease of viewing.

**4 Conclusions** We present a model to study the changes in reflectance induced by the displacement of single atomic monolayers in a crystalline semiconductor slab, and apply our model on the Si(111)(1×1):H system. We find that the normal incidence reflectance increases with respect to the relaxed system for compressive and tensile strain, but only for incident photon energies above $\sim$ 2.0 eV. For our example system, we also found that most of the linear optical response comes from elongated bonds, rather than from compressed ones. The magnitude of our calculated results is within what is experimentally measurable using lock-in techniques.

Although our scheme for displacing the atoms is a simplified depiction of a real strain wave propagating through a material, it constitutes a first building block for modeling more realistic systems. This model can be readily extended to consider a superposition of displaced atomic layers, which would allow for modeling different strain profiles. Our supercell method is also very flexible, and can easily accommodate the inclusion of defects or deformities in the crystalline lattice. Furthermore, a layer-by-layer analysis of the optical reflectance can be readily studied within our current framework [4]. Ultimately, we consider that our *ab initio* approach is an attractive option for modeling the optoelectronic properties of a material undergoing atomic disorder, and that extending our model could

help understand results from experimental techniques such as CAP spectroscopy or RAS.

**Acknowledgements** We acknowledge useful discussions with N. Tolk and Lucero Cano. Bernardo S. Mendoza acknowledges partial support from CONACYT-México Grant 153930. Ramón Carriles and Bernardo S. Mendoza thank the *Red Nanociencias y Nanotecnología* of México for partial financial support.

## References

[1] C. D. Hogan and C. H. Patterson, Phys. Rev. B **57**(23), 14843 (1998).
[2] M. Palummo, G. Onida, R. Del Sole, and B. S. Mendoza, Phys. Rev. B **60**(4), 2522–2527 (1999).
[3] C. Hogan, R. Del Sole, and G. Onida, Phys. Rev. B **68**(3), 035405 (2003).
[4] B. S. Mendoza, F. Nastos, N. Arzate, and J. Sipe, Phys. Rev. B **74**(7), 075318 (2006).
[5] M. Palummo, N. Witkowski, O. Pluchery, R. Del Sole, and Y. Borensztein, Phys. Rev. B **79**(3), 035327 (2009).
[6] N. Tancogne-Dejean, B. S. Mendoza, and V. Véniard, Phys. Rev. B **90**(3), 035212 (2014).
[7] N. Tancogne-Dejean, C. Giorgetti, and V. Véniard, Phys. Rev. B **92**(24), 245308 (2015).
[8] C. H. Thomsen, J. Strait, Z. Vardeny, H. J. Maris, J. Tauc, and J. J. Hauser, Phys. Rev. Lett. **53**(10), 989 (1984).
[9] C. H. Thomsen, H. T. Grahn, H. J. Maris, and J. Tauc, Phys. Rev. B **34**(6), 4129 (1986).
[10] H. T. Grahn, H. J. Maris, and J. Tauc, IEEE J. Quant. Electron. **25**(12), 2562–2569 (1989).
[11] H. N. Lin, R. J. Stoner, H. J. Maris, and J. Tauc, J. Appl. Phys. **69**(7), 3816–3822 (1991).
[12] T. Pfeifer, W. Ktt, H. Kurz, and R. Scholz, Phys. Rev. Lett. **69**(22), 3248 (1992).
[13] C. Rossignol, J. M. Rampnoux, M. Perton, B. Audoin, and S. Dilhaire, Phys. Rev. Lett. **94**(16) (2005).
[14] H. Park, X. Wang, S. Nie, R. Clinite, and J. Cao, Phys. Rev. B **72**(10) (2005).
[15] S. Wu, P. Geiser, J. Jun, J. Karpinski, J. R. Park, and R. Sobolewski, Appl. Phys. Lett. **88**(4), 041917 (2006).
[16] O. Matsuda, O. B. Wright, D. H. Hurley, V. E. Gusev, and K. Shimizu, Phys. Rev. Lett. **93**(9) (2004).
[17] J. K. Miller, J. Qi, Y. Xu, Y. J. Cho, X. Liu, J. K. Furdyna, I. Perakis, T. V. Shahbazyan, and N. H. Tolk, Phys. Rev. B **74**(11) (2006).
[18] Y. C. Wen, L. C. Chou, H. H. Lin, V. Gusev, K. H. Lin, and C. K. Sun, Appl. Phys. Lett. **90**(17), 172102 (2007).
[19] Y. Xu, J. Qi, J. Miller, Y. J. Cho, X. Liu, J. K. Furdyna, T. V. Shahbazyan, and N. H. Tolk, physica status solidi (c) **5**(8), 2632–2636 (2008).
[20] P. Babilotte, P. Ruello, D. Mounier, T. Pezeril, G. Vaudel, M. Edely, J. M. Breteau, V. Gusev, and K. Blary, Phys. Rev. B **81**(24) (2010).
[21] F. Hudert, A. Bartels, T. Dekorsy, and K. Köhler, J. Appl. Phys. **104**(12), 123509 (2008).
[22] D. Lim, R. D. Averitt, J. Demsar, A. J. Taylor, N. Hur, and S. W. Cheong, Appl. Phys. Lett. **83**(23), 4800–4802 (2003).
[23] I. Bozovic, M. Schneider, Y. Xu, R. Sobolewski, Y. H. Ren, G. Lpke, J. Demsar, A. J. Taylor, and M. Onellion, Phys. Rev. B **69**(13) (2004).
[24] P. Ruello, S. Zhang, P. Laffez, B. Perrin, and V. Gusev, Phys. Rev. B **79**(9) (2009).
[25] P. Ruello, T. Pezeril, S. Avanesyan, G. Vaudel, V. Gusev, I. C. Infante, and B. Dkhil, Appl. Phys. Lett. **100**(21), 212906 (2012).
[26] L. Y. Chen, J. C. Yang, C. W. Luo, C. W. Laing, K. H. Wu, J. Y. Lin, T. M. Uen, J. Y. Juang, Y. H. Chu, and T. Kobayashi, Appl. Phys. Lett. **101**(4), 041902 (2012).
[27] V. Gusev, A. M. Lomonosov, P. Ruello, A. Ayouch, and G. Vaudel, J. Appl. Phys. **110**(12), 124908 (2011).
[28] O. Matsuda and O. B. Wright, J. Opt. Soc. Am. B **19**(12), 3028–3041 (2002).
[29] H. T. Grahn, D. A. Young, H. J. Maris, J. Tauc, J. M. Hong, and T. P. Smith, Appl. Phys. Lett. **53**(21), 2023–2024 (1988).
[30] H. T. Grahn, H. J. Maris, J. Tauc, and K. S. Hatton, Appl. Phys. Lett. **53**(23), 2281–2283 (1988).
[31] H. Tanei, N. Nakamura, H. Ogi, M. Hirao, and R. Ikeda, Phys. Rev. Lett. **100**(1) (2008).
[32] J. Qi, J. A. Yan, H. Park, A. Steigerwald, Y. Xu, S. N. Gilbert, X. Liu, J. K. Furdyna, S. T. Pantelides, and N. H. Tolk, Phys. Rev. B **81**(11) (2010).
[33] T. C. Zhu, H. J. Maris, and J. Tauc, Phys. Rev. B **44**(9), 4281 (1991).
[34] B. C. Daly, K. Kang, Y. Wang, and D. G. Cahill, Phys. Rev. B **80**(17) (2009).
[35] G. Tas, J. J. Loomis, H. J. Maris, A. A. Bailes, and L. E. Seiberling, Appl. Phys. Lett. **72**(18), 2235–2237 (1998).
[36] A. Steigerwald, A. B. Hmelo, K. Varga, L. C. Feldman, and N. H. Tolk, J. Appl. Phys. **112**(1), 013514 (2012).
[37] A. Steigerwald, Y. Xu, J. Qi, J. Gregory, X. Liu, J. K. Furdyna, K. Varga, A. B. Hmelo, G. Lüpke, L. C. Feldman, and N. H. Tolk, Appl. Phys. Lett. **94**(11), 111910 (2009).
[38] J. Gregory, A. Steigerwald, H. Takahashi, A. Hmelo, and N. H. Tolk, Appl. Phys. Lett. **101**(18), 181904 (2012).
[39] A. Baydin, H. Krzyzanowska, M. Dhanunjaya, S. V. S. Nageswara Rao, J. L. Davidson, L. C. Feldman, and N. H. Tolk, APL Photonics **1**(3), 036102 (2016).
[40] D. Mounier, E. Morozov, P. Ruello, J. M. Breteau, P. Picart, and V. Gusev, Eur. Phys. J. Spec. Top. **153**(1), 243–246 (2008).
[41] D. Mounier, P. Picart, P. Babilotte, P. Ruello, J. M. Breteau, T. Pézeril, G. Vaudel, M. Kouyaté, and V. Gusev, Opt. Express **18**(7), 6767–6778 (2010).
[42] H. M. Lawler, A. Steigerwald, J. Gregory, H. Krzyzanowska, and N. H. Tolk, Mater. Res. Express **1**(2), 025701 (2014).
[43] S. M. Anderson and B. S. Mendoza, Physical Review B **94**(11), 115314 (2016).
[44] S. M. Anderson and B. S. Mendoza, Frontiers in Materials **4**, 12 (2017).
[45] R. Del Sole, Reflectance spectroscopy – Theory, in: Photonic Probes of Surfaces, edited by P. Halevi, No. 2 in Electromagnetic waves (Elsevier, Amsterdam; New York, 1995), pp. 131–174.
[46] S. M. Anderson, N. Tancogne-Dejean, B. S. Mendoza, and V. Véniard, Phys. Rev. B **91**(7), 075302 (2015).

[47] X. Gonze, B. Amadon, P. M. Anglade, J. M. Beuken, F. Bottin, P. Boulanger, F. Bruneval, D. Caliste, R. Caracas, M. Côté, T. Deutsch, L. Genovese, P. Ghosez, M. Giantomassi, S. Goedecker, D. R. Hamann, P. Hermet, F. Jollet, G. Jomard, S. Leroux, M. Mancini, S. Mazevet, M. J. T. Oliveira, G. Onida, Y. Pouillon, T. Rangel, G. M. Rignanese, D. Sangalli, R. Shaltaf, M. Torrent, M. J. Verstraete, G. Zerah, and J. W. Zwanziger, Comp. Phys. Commun. **180**(12), 2582–2615 (2009).
[48] The ABINIT code is a common project of the Université Catholique de Louvain, Corning Incorporated, and other contributors (URL http://www.abinit.org).
[49] H. Landolt, R. Börnstein, K. H. Hellwege, J. B. Goodenough, M. Schulz, H. Weiss, and O. Madelung, Numerical data and functional relationships in science and technology, New Series: Group III, Crystal and Solid State Physics, Vol. 17, Semiconductors (Springer, Berlin, 1984).
[50] J. E. Ortega and F. J. Himpsel, Phys. Rev. B **47**(4), 2130 (1993).
[51] F. Bruneval, N. Vast, and L. Reining, Phys. Rev. B **74**(4), 045102 (2006).
[52] Y. Li and G. Galli, Phys. Rev. B **82**(4), 045321 (2010).